BIOCHEMISTRY
including biophysical chemistry & molecular biology

Article

pubs.acs.org/biochemistry

Two ZnF-UBP Domains in Isopeptidase T (USP5)

George V. Avvakumov,[†,‡,#] John R. Walker,[†,#] Sheng Xue,[†,‡] Abdellah Allali-Hassani,[†] Abdalin Asinas,[†,‡] Usha B. Nair,[†,‡] Xianyang Fang,[§] Xiaobing Zuo,[∥] Yun-Xing Wang,[§] Keith D. Wilkinson,[⊥] and Sirano Dhe-Paganon*[,†,‡]

[†]Structural Genomics Consortium and [‡]Department of Physiology, University of Toronto, 101 College St., Toronto, ON M5G 1L7, Canada

[§]Protein-Nucleic Acid Interactions Section, Structural Biophysical Laboratory, 1050 Boyles St., National Cancer Institute, Frederick, Maryland 21702, United States

[∥]X-ray Science Division, Argonne National Laboratory, 9700 South Cass Avenue, Argonne, Illinois 60439, United States

[⊥]Department of Biochemistry, Emory University School of Medicine, Atlanta, Georgia 30322, United States

Supporting Information

ABSTRACT: Human ubiquitin-specific cysteine protease 5 (USP5, also known as ISOT and isopeptidase T), an 835-residue multidomain enzyme, recycles ubiquitin by hydrolyzing isopeptide bonds in a variety of unanchored polyubiquitin substrates. Activation of the enzyme's hydrolytic activity toward ubiquitin-AMC (7-amino-4-methylcoumarin), a fluorogenic substrate, by the addition of free, unanchored monoubiquitin suggested an allosteric mechanism of activation by the ZnF-UBP domain (residues 163−291), which binds the substrate's unanchored diglycine carboxyl tail. By determining the structure of full-length USP5, we discovered the existence of a cryptic ZnF-UBP domain (residues 1−156), which was tightly bound to the catalytic core and was indispensable for catalytic activity. In contrast, the previously characterized ZnF-UBP domain did not contribute directly to the active site; a paucity of interactions suggested flexibility between these two domains consistent with an ability by the enzyme to hydrolyze a variety of different polyubiquitin chain linkages. Deletion of the known ZnF-UBP domain did not significantly affect rate of hydrolysis of ubiquitin-AMC and suggested that it is likely associated mainly with substrate targeting and specificity. Together, our findings show that USP5 uses multiple ZnF-UBP domains for substrate targeting and core catalytic function.

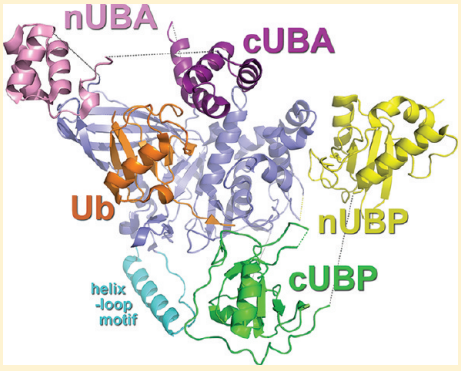

Regulation of intracellular proteins through their post-translational ubiquitylation involves two antagonistic enzyme classes: E3 ligases and ubiquitin hydrolases, the former catalyzing conjugation of ubiquitin, a 76-residue phylogenetically conserved protein, to substrate lysines with the formation of isopeptide bonds and the latter catalyzing hydrolysis of these bonds. Ubiquitylation has multiple effects on substrate proteins, including effects on their localization, enzymatic efficiency, and interaction with other proteins. Ubiquitin interacts with numerous binding partners, three dozen of which have so far been characterized in high-resolution complex structures. The ubiquitin-associated (UBA) domain, for example, is an ∼45 amino acid long three-helix bundle with a hydrophobic surface centered around a conserved (M/L)G(F/Y) motif that recognizes ubiquitin. This domain is present in over 50 predominantly ubiquitin-related human proteins, including a deubiquitylating enzyme, USP5, also known as isopeptidase T (IsoT).

With seven surface lysines, ubiquitin itself is also a substrate of ubiquitylation and may form long chains. Lys48-linked polyubiquitin chains have been best characterized; these are specifically recognized by the 26S proteasome for full degradation of the attached protein substrate. Other linkages have roles that may be independent of proteasomal degradation; Lys11 and -29 linkages, for example, are implicated in lysosomal and aggresomal degradation, and Lys63 linkages are implicated in protein localization and nonproteolytic regulation of signaling pathways.[1,2] Other linkages, including Lys6, -27, and -33, have been detected to some degree using various mass-spectroscopic techniques but are less understood.[3]

The structure of different chain types in solution is not well-defined. In the crystalline state, there are significant differences in noncovalent interactions between adjacent core domains, but whether these are relevant is unclear.[4] Structures of ubiquitin chains can be characterized statistically with methods that take into account the flexibility of the short ubiquitin tail, and a number of conformational ensembles have been described to

Received: June 2, 2011
Revised: January 23, 2012
Published: January 23, 2012

dx.doi.org/10.1021/bi200854q | *Biochemistry* 2012, 51, 1188−1198

date.[5] Polyubiquitin-binding proteins therefore likely have evolved to discriminate between the different ensembles.

About 100 genes in the human genome express enzymes with deubiquitylation activity. While most of these proteases catalyze substrate-specific (also known as substrate-anchored) deubiquitylation, USP5 and possibly its closest paralog USP13 hydrolyze unanchored polyubiquitin chains.[6] An important source of unanchored polyubiquitin chains is at the proteasome, where ubiquitin chains are released intact. These chains are recycled back to monoubiquitin by USP5. USP5 has been shown to cleave at least five types of polyubiquitin linkages, including K6, K29, K48, and K63 as well as linear polyubiquitin chains. The latter represents the pro form of ubiquitin, which consists of nine continuous ubiquitin domains derived from the corresponding open reading frame. To recognize these substrates, the USP5 catalytic domain requires the help of multiple substrate targeting domains. We have already shown that USP5 has at least four ubiquitin binding sites; the proximal (S1) ubiquitin moiety is bound by the ZnF UBP domain, the second (S1) by the catalytic USP domain, the third (S2) by the second UBA, and the fourth (S3) by the first UBA domain.[7]

It was previously observed that the addition of free monoubiquitin increased the efficiency of hydrolysis of ubiquitin-AMC and that possibly the ZnF-UBP contributes to the basic catalytic machinery upon binding free monoubiquitin.[8] To test this model, we determined the structure of full-length USP5 and show that the ZnF-UBP does not interact closely with the active site. Instead, it is tethered within the vicinity of the active site in order to accommodate a variety of substrates with different structural ensembles. Our serendipitous discovery of an additional domain in USP5, whose molecular function is unknown but which we show is necessary for catalysis, prompted us to selectively delete the ZnF-UBP domain and show that the ZnF-UBP domain did not significantly contribute to hydrolysis of Ub-AMC, and by extension, to the hydrolysis of polyubiquitin substrates. The ZnF-UBP domain therefore contributes mainly toward substrate affinity and specificity.

MATERIALS AND METHODS

Cloning and Purification. Full-length ubiquitin specific peptidase 5 (USP5, also known as isopeptidase T) was cloned using a cDNA template from MGC (AU25-C3, pOTB7) into the pET28a-LIC vector (GenBank, EF442785) using the In-Fusion CF Dry-Down PCR Cloning Kit (Clontech, 639605). Competent BL21 (DE3) cells (Invitrogen C6000-03) were transformed and grown using the LEX system (Harbinger BEC) at 37 °C in 2 L bottles (VWR 89000-242) containing 1800 mL of TB (Sigma T0918) supplemented with 150 mM glycerol, 100 μg/mL kanamycin, and 600 μL of antifoam 204 (Sigma A-8311). When OD(600) ∼ 6 was reached, the temperature was reduced to 15 °C, and 1 h later protein expression was induced with 100 μM IPTG (BioShop IPT001) and the culture was incubated overnight (16 h) at 15 °C. Cell pellets were collected by centrifugation (12227*g*, 20 min), frozen, and stored at −80 °C. After resuspension in 30 mL per liter of bacterial culture of lysis buffer (10 mM Tris(pH 8.0), 0.5 M NaCl, 5% glycerol, 2 mM imidazole, 1 mM β-mercaptoethanol, 0.1 μM phenylmethylsulfonyl fluoride (PMSF)), cells were lysed using a Microfluidics M110-EH microfluidizer at 18 000 psi. The cleared lysate was loaded onto a 3 mL TALON metal-affinity resin column (BD Biosciences) at 4 °C. The column was washed with 10 mL of wash buffer A (10 mM Tris(pH 8.0), 0.5 M NaCl, 5% glycerol, 10 mM imidazole, 1 mM β-mercaptoethanol), 10 mL of wash buffer B (wash buffer A supplemented with 0.05% Tween 20), and 10 mL of wash buffer A. The protein was eluted with 6 mL of elution buffer (10 mM Tris(pH 8.0), 0.5 M NaCl, 5% glycerol, 200 mM imidazole, 1 mM β-mercaptoethanol). The expressed protein at this stage included residues 1−835 with an additional 19 residues (MGSSHHHHHHSSGLVPRGS) from the expression tag. The N-terminal His-tag was removed by overnight incubation of the protein with thrombin (1 unit/mg protein) at 4 °C. The protein was further purified by gel filtration on a HighLoad 16/60 Superdex 200 column (GE Healthcare) using gel filtration buffer (20 mM Tris(pH 8.0), 0.5 M NaCl, 5% glycerol, 2 mM dithiothreitol). Fractions containing protein corresponding to the USP5 peak were pooled and concentrated by ultrafiltration. The yield of the protein was 5 mg per liter of bacterial culture.

Modification with Suicide Substrate. The suicide substrate, ubiquitin(1−75)-bromoethylamide, was prepared using a scaled-up and modified protocol.[9] Residues 1−75 of mammalian ubiquitin were cloned from a Mammalian Genome Collection template (rps27a.BC001392.MGC.AU6-F3.pOTB7) into the multiple cloning sites region of pTYB2 vector (New England Biolabs, N6702S) using NdeI and *Sma*I restriction sites after the addition of the corresponding sites by PCR to the 5′ and 3′ ends of the cDNA, respectively. Competent BL21 (DE3) cells were transformed and grown as above in TB medium supplemented with 100 μg/mL ampicillin instead of kanamycin. For protein purification, the bacterial cells from 1 L of culture were suspended in 50 mL of Ub-MESNA lysis buffer (20 mM Hepes, 50 mM NaOAc, 75 mM NaCl, final pH 6.5), and cells were lysed using a Microfluidics M110-EH microfluidizer at 18 000 psi. Cell debris was removed by centrifugation at 20000*g* for 30 min. The clarified lysate was mixed with chitin beads (New England Biolabs, S6651L) equilibrated with lysis buffer (2.5 mL of beads per 50 mL of lysate). The suspension was incubated with constant stirring for 2 h at 37 °C and poured into an open-end column. The column was drained, and the beads were washed with 10 volumes of lysis buffer. The column was then filled with 1 volume of 100 mM 2-mercaptoethanesulfonic acid (MESNA, Sigma M1511), closed tightly, gently shaken to resuspend the resin in the MESNA solution, plugged, and left overnight (16 h) at room temperature. The column was then opened, and the eluate was collected and combined with additional washing of the column with 2 volumes of MESNA solution. The combined eluate, containing ubiquitin(1−75)-MESNA thiol ester, was concentrated to a final volume of ∼5 mL and loaded onto a HighLoad 16/60 Superdex 200 column equilibrated with lysis buffer. Gel-filtration fractions were collected and analyzed by LC/MC, and those containing purified ubiquitin(1−75)-MESNA thiol ester were combined, divided into 1 mL aliquots, frozen with liquid nitrogen, and stored at −80 °C. The yield of the thiol ester was ∼7 mg per liter of bacterial culture.

In order to prepare ubiquitin(1−75)-bromoethylamide, 150 mg of 2-bromoethylamine hydrobromide (Sigma B65705) was dissolved in 1 mL of ubiquitin(1−75)-MESNA thiol ester solution (3 mg/mL), and 200 μL of 2 M NaOH was added. The reaction mixture was incubated for 20 min at room temperature and dialyzed against 4 L of dialysis buffer NaOAc (pH 5.5) for 2 h at 4 °C using a Slide-A-Lyzer with molecular-weight cutoff limit of 3500 (Pierce). The pH of the dialyzed

solution was adjusted to 7.5, and NaCl was added to a final concentration of 0.5 M before use. A mass of 32 mg of USP5 was incubated with 10-fold molar excess of ubiquitin(1−75)-bromoethylamide for 1 h at room temperature (21 °C). The covalent complex was purified by gel-filtration chromatography (as USP5 above) and concentrated by ultrafiltration to a final concentration of 25 mg/mL. The concentrated protein was stored on ice. Coomassie-stained SDS-PAGE showed that the product was pure and analysis by LC/MS (Agilent 1100 Series) showed that its molecular weight corresponded to the calculated molecular weight of the USP5 construct, with N-terminal His-tag removed, covalently linked to ubiquitin 1−75 through an ethylene spacer.

Crystallization. Crystals of the covalent ubiquitin complex of USP5 were grown at 298 K using the hanging drop method by mixing equal volumes of protein solution (25 mg/mL) and crystallization buffer (1.45 M NH_4SO_4, 0.1 M BisTris(pH 6.5), 0.2 M NaOAc, 5% ethylene glycol, and 1 mM DTT). Crystals were cryoprotected by immersion in Paratone N in paraffin oil 30% (v/v) and placed in liquid nitrogen.

Structure Determination. Diffraction data from a crystal of the USP5−ubiquitin complex were collected at beamline 23-ID-B of the GM/CA-CAT at the Advanced Photon Source (Argonne National Laboratory). The data set was integrated and scaled using the HKL2000 program suite.[10] The structure was solved by molecular replacement techniques using the program PHASER and search model PDB entries 2IBI and 2G43.[11] After improvement of the phases through model building and refinement, models from each of PDB entries 2DAG and 2DAK were positioned. Iterative model building using the graphics program Coot and TLS and restrained refinement using REFMAC5 led to a model with an R factor of 23.1% (Rfree 27.8%) for data between 34.9 and 2.80 Å.[11,12] Medium weight positional and thermal restraints were applied between NCS copies. Initial TLS parameters were obtained from the TLSMD web server.[13] Statistics of data collection, processing, and refinement are provided in Table 1.

SAXS Data Collection and Analysis. SAXS data sets for apo USP5, in 20 mM Tris(pH 8.0), 500 mM NaCl, 2 mM DTT, and 2.5% glycerol, were collected at beamline 12-ID-B of the Advanced Photon Source, Argonne National Laboratory. The energy of the X-ray beam was 12 keV (wavelength λ = 1.033 Å), and the distance from the sample to detector (PILATUS 2M, Dectris Ltd.) was 2 m, covering a scattering vector range ($q = 4\pi \sin\theta/\lambda$) from 0.007 to 0.66 $Å^{-1}$, as determined by the scattering profile of silver behenate. A total of 20 frames of two-dimensional images were recorded for each buffer or sample using a flow cell, with the exposure time of 5 s for each frame and the sleep time of 1 s between each frame, to reduce radiation damage and get good statistics. The 2D images were reduced to one-dimensional scattering profiles using Matlab scripts on site. The scattering profile of a sample solute was calculated by subtracting the buffer contribution from the sample−buffer profile using the program PRIMUS.[14] The experimental radius of gyration (R_g) and the forward scattering intensity $I(0)$ were calculated from data at low q values in the range of $qR_g < 1.3$, using the Guinier approximation: $\ln I(q) \approx \ln(I(0)) - R_g^2 q^2/3$. The R_g derived by this reciprocal method for three concentrations (1.1, 2.2, and 4.3 mg/mL) samples were 38.1, 38.2, and 38.2 Å, respectively and no concentration-dependent systematic differences in R_g were observed, indicating the absence of intermolecular or oligomeric interactions. The forward scattering $I(0)$ obtained from Guinier fits can be related to the molecular weight of the sample (MW_p) by comparing with a molecular weight standard of known concentration c_{ST} and molecular weight MW_{ST} by a simple formula: $MW_p = (I(0)_p c_{ST} MW_{ST})/(c_p I(0)_{ST})$, where $I(0)_p$ and $I(0)_{ST}$ are the forward scattering intensities for the sample and standard protein, respectively, and c_p is the sample concentration. The pair distance distribution function (PDDF), $p(r)$, and the maximum dimension of the protein, D_{max}, in real space were calculated with the indirect Fourier transform program GNOM.[15] The theoretical scattering intensity of the atomic structure model was calculated and fitted to the experimental scattering intensity using CRYSOL.[16]

Table 1. Data Collection and Refinement Statistics

data set	
PDB code	3IHP
space group	$P2_12_12_1$
unit cell a, b, c	68.29, 188.85, 207.86
beamline	APS 23-ID-B
wavelength	0.97918
resolution	35.0−2.80
unique reflections	66229
data redundancy[a]	5.4 (5.4)
completeness	98.0% (94.6)
I/sig$I$	17.1 (2.0)
R_{sym}	0.101 (0.845)
$R_{p.i.m.}$	0.048 (0.390)
refinement	
resolution	34.9−2.80
reflections used	62592
all atoms (hetero, solvent)	11800 (41)
R_{work}/R_{free}[b]	22.4/27.6%
rmsd bond length, Å	0.011
rmsd bond angle, deg	1.3
mean B factor, $Å^2$	73.95
Ramachandran plot, %	
favored	96.9
allowed	100
disallowed	0

[a]Highest resolution shell shown in parentheses. [b]R_{free} calculated with 5% of the data.

***Ab Initio* Modeling.** Low-resolution *ab initio* shape reconstructions were performed with the programs DAMMIN, which generates models represented by an ensemble of densely packed beads,[17] using scattering data within the q range of 0.007−0.30 $Å^{-1}$. An alternative *ab initio* model was generated using the program GASBOR[18] which models the particle in solution as a protein-like assembly of dummy residues against the scattering data with the q range of 0.007−0.65 $Å^{-1}$. A total of 32 independent runs for both programs were performed, and the resulting models were subjected to averaging by DAMAVER[19] and were superimposed by SUPCOMB[20] based on the normalized spatial discrepancy (NSD) criteria and were filtered using DAMFILT to generate the final model.

Rigid-Body Modeling. Rigid body molecular modeling was done with the atomic models of the individual domains of USP5 using BUNCH program.[21] This program combines rigid body and *ab initio* modeling of multidomain proteins linked by flexible linkers (for which were treated as dummy residues), employing a simulated annealing protocol to refine the position and orientation of rigid domains against the experimental scattering data.

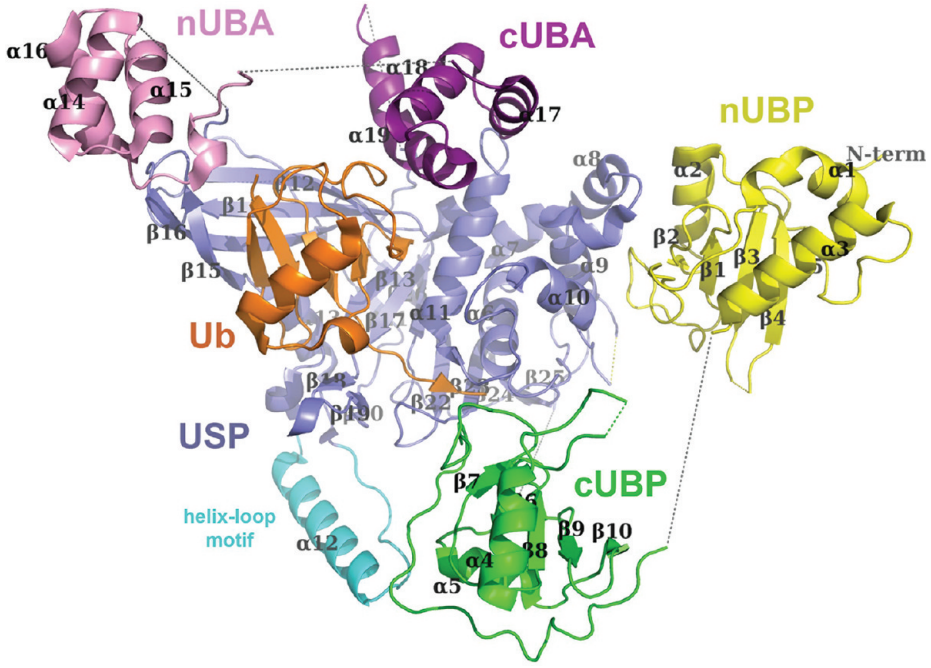

Figure 1. USP5-Ub complex structure. Ribbon representation of the FL USP5 structure is shown with nUBP colored yellow, cUBP colored green, nUBA colored violet, and cUBA colored magenta. Ubiquitin, covalently attached to the catalytic cysteine, is colored orange. Peptide regions that were not modeled are represented as dashed lines. Secondary structure elements are labeled.

Flexibility Assessment. The flexibility of USP5 was analyzed using the program EOM.[22] A genetic algorithm was employed to optimize an ensemble of coexisted conformers that best describe the protein from an initial pool of 10 000 random conformers. This was done by minimizing the discrepancy between the average scattering profile of the ensemble and the experimental scattering data, providing a quantitative characterization of the flexibility of a protein and analysis of the size distribution of possible conformers.

Ub-AMC Hydrolysis Assay. Enzymatic reactions were conducted in assay buffer containing 50 mM Hepes(pH 7.5), 0.01% Tween 20, and 10 mM DTT. All enzymes and substrate were diluted in assay buffer, and reactions were performed in a 50 μL total volume at 20 °C in 384-well plates. AMC fluorescence was measured at 460 nm (excitation wavelength of 360 nm) using a Biotek Synergy 2 plate reader. For enzymatic parameter determination, wild-type full-length USP5 (1−835), ΔnUBP USP5 (173−835), and full-length USP5 F32S/F34S double mutant were used at 2, 20, and 400 nM, respectively. Ub-AMC substrate (Boston Biochem) was used at concentrations ranging from 10 nM to 10 μM, keeping the DMSO concentration at 4% (v/v) in all assays. K_m and k_{cat} values were obtained by fitting the data into a hyperbolic function using Sigma Plot 9.

Mass Spectrometry. Mass-spectrometric assessment of the enzymatic activity of USP5 variants was conducted in 10 μL of 1 mg/mL substrate solution (either K11-, K48-, or K63-linked diubiquitin or K48- or K63-linked tretraubiquitin, all from Boston Biochem) mixed with 1 μL of enzyme solution (10 nM final enzyme concentration in the reaction mixture) and 50 μL of buffer (20 mM Tris(pH 7.5), 150 mM NaCl, 2 mM DTT). The reaction mixtures were incubated at 23 °C, and 10 μL aliquots were taken at 1, 5, 10, and 20 min after the start of the reaction, mixed with 150 μL of 0.1% (v/v) formic acid to stop the reaction and analyzed using LC/MSD TOF model G1969A mass-spectrometer equipped with 1100 Series HPLC (Agilent).

RESULTS AND DISCUSSION

To determine the basis of a putative allosteric activation mechanism by the ZnF-UBP, we solved the full-length USP5 structure. Recombinant full-length human USP5/ISOT (residues 1−835) was purified from bacteria, inhibited with a ubiquitin-based suicide substrate and crystallized at 20 °C. A 2.8 Å resolution data set was collected yielding a structure after phases were obtained by molecular replacement (covalent ubiquitin-USP2 complex (PDB code 2IBI) and the USP5 ZnF-UBP domain (PDB code 2G43)) with good crystallographic statistics (Table 1). Two molecules of USP5 and their covalently attached ubiquitin substrates were present in the asymmetric unit, with a root-mean-square deviation (rmsd) of 0.99 Å over all Cα positions.

USP5 was thought to be composed of five individual domains, including the ubiquitin diglycine-binding ZnF-UBP domain (residues 173−283, herein referred to the cUBP) and two UBA domains between residues 634−684 and 698−749, which are inserted within the catalytic domain (Figure S1). We discovered a novel domain at the amino-terminus, which will be described below. Clear electron density was not observed for residues 76−117, 156−173, 223−225, 283−319, 388−410, 617−634, 684−698, and 749−769 (Figure 1). Except for the first, these missing segments corresponded to interdomain linkers, which were presumably disordered in our structure as mass-spectrometry results did not indicate evidence of protein sample degradation prior to crystal growth. Absence of linker electron density introduced an element of uncertainty regarding domain connectivity. Because USP5 was monomeric in solution (see below), connectivities that supported a domain-swapping model were excluded. Final chain assignment was based on the shortest distances between adjacent domains and was in agreement with the greatest surface interaction with the catalytic domain (Figure 1 and Figure S2). Ubiquitin was

dx.doi.org/10.1021/bi200854q | *Biochemistry* 2012, 51, 1188−1198

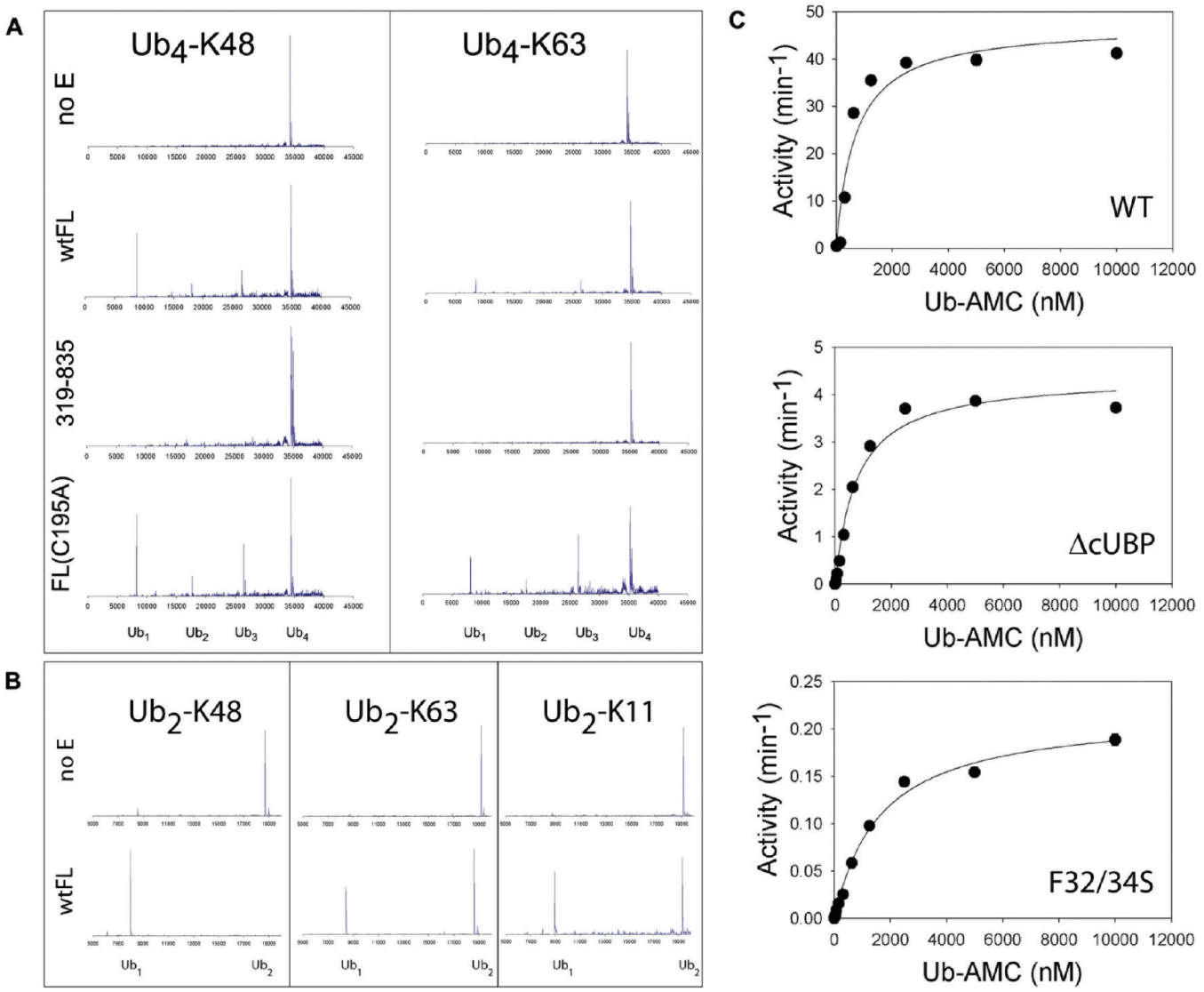

Figure 2. Biochemical assays. Mass-spectrometry results of reaction products (5 min at 23 °C) using tetraubiquitin (A) and diubiquitin (B) isomers are shown. Substrates are listed above and enzyme variants used on the left. Positions of substrates and products are shown below. (C) Shown are substrate-dependent initial rates determined using the fluorescence-based Ub-AMC assay, with Michaelis–Menten kinetic parameters listed in Table 2.

bound by the catalytic domain, covalently attached via an ethylene bridge to the catalytic cysteine.

Catalytic Domain. As with other USPs, the catalytic core of USP5 was composed of the papain-like fold with an extended active site (Figure 1). The papain-like core was composed of a helical lobe (α6–α11) abutting a torn β-sheet lobe (β13, 17, 26, 22–25). The interface between these lobes formed the active site, where the catalytic cysteine (Cys335) of the triad was attached to one of the helices in the helical lobe (α6) and the catalytic histidine and aspartate was attached to the β-sheet lobe (β23 and 24). The active site extension (also referred to as the fingers lobe/domain) was mostly an insertion between the helical lobe and the β-sheet; the extension formed a β-sheet (β11, 12, 15, and 16) and was contiguous but orthogonal to the papain-like β-sheet lobe, and it was capped by a zinc-ribbon-like subdomain that, like USP7, did not bind zinc.

The substrate binding pocket of USP5 was occupied by ubiquitin, in a manner similar to Ub complex structures of USP2, USP7, USP14, and USP21 (Figure 1). A slight rotation of the fingers lobe of USP5 and protrusion of a phenylalanine and a tryptophan residue from BL2 (β18–β19) was associated with a slight rotation of the bound ubiquitin. As with other complex structures, the ubiquitin β-sheet formed a β-sandwich with the fingers lobe that buried Phe4 and formed a number of hydrogen-bonding pairs around Phe4. But, the USP5-ubiquitin β-sandwich contained a salt bond (Glu64-Lys478) not seen in other complex structures (Figure S3). Water molecules, thought to be important for the interaction between the enzyme and ubiquitin,[23] were also observed at the interface between ubiquitin and the catalytic domain in our complex structure. Finally, although the binding pocket for the substrate's diglycine motif is highly conserved compared with other mammalian structures, the USP5 active site diverged regarding interactions with Arg74 of Ub, forming a unique salt bridge with Glu427. Therefore, interaction between USP5 and the proximal (Figure S1) ubiquitin was globally canonical; local variances may account for differences in substrate chain specificity.

dx.doi.org/10.1021/bi200854q | *Biochemistry* 2012, 51, 1188–1198

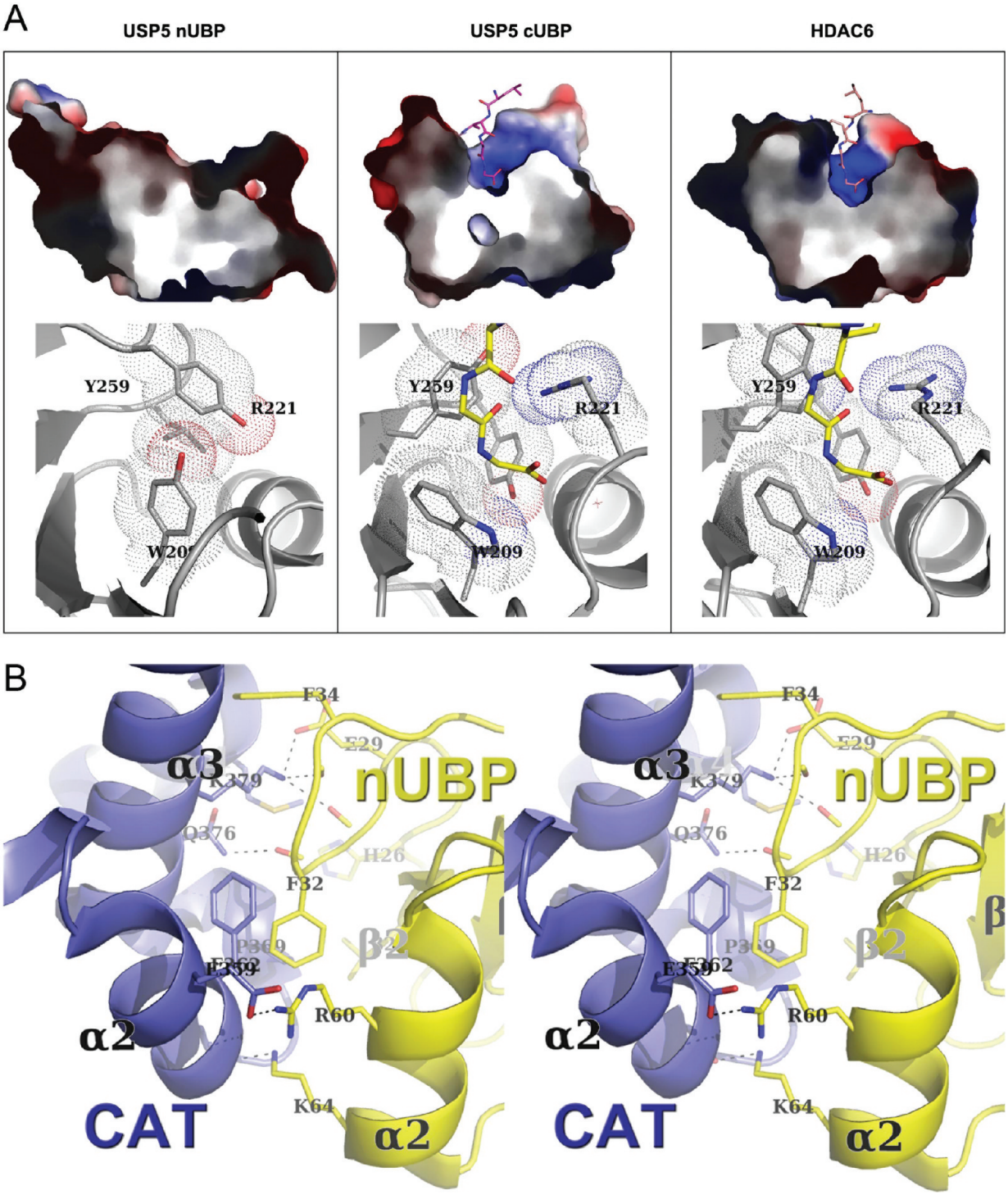

Figure 3. The nUBP domain. (A) Cutaway view of an electrostatic surface representation (−70 to +70 kT/e) of the USP5 nUBP, cUBP, and HDAC6 UBP. Bound ubiquitin tails in cUBP and HDAC6 UBP are shown in stick format. A close-up view of the corresponding ligand binding cleft is shown below the surface representation. Prominent UBP side chains are labeled and shown in stick format and their van der Waals radii are shown as dots. (B) The catalytic−nUBP interface is shown stereoscopically, with labeled domains as ribbons and interacting, labeled residues in stick format. Hydrogen and ionic bonds are shown as black dashed lines.

The Helix−Loop Motif. As with USP2, 8, 14, and 21, USP5 contained an insertion segment, composed of an α helix, a hydrogen-bonded turn, and an extended polypeptide running alongside the helix (Figure S4). The function of this segment was unknown. While this motif is inserted after α11 in USP2, 8, and 21, it is inserted prior to β22 in USP14 and after β13 in USP5 (Figure S4). The USP5 helix-loop motif extended into solution in a direction opposite to the fingers. It was well-ordered, despite making only a few crystal packing contacts at its tip. A number of hydrophobic residues packed between the helix and the extended peptide probably to stabilize the conformation of this segment. The absence of sequence similarity with the ubiquitin interacting motif (UIM) suggested that it was unlikely to bind ubiquitin. This was confirmed by

dx.doi.org/10.1021/bi200854q | *Biochemistry* 2012, 51, 1188−1198

the inability of HIS-tagged, HisLink-immobilized helix-loop peptides of USP5 to bind GST-tagged ubiquitin (Figure S5).

UBA Domains. The two USP5 UBA domains, designated nUBA and cUBA, adopted the canonical fold and aligned well with one another, with an rmsd of 2.8 Å over 38 Cα positions (Figure S6). Exemplified by the ubiquilin−ubiquitin complex structure, a hydrophobic patch on α1 and α3 helices of many UBA domains mediates ubiquitin binding.[24,25] The corresponding patches in nUBA and cUBA were conserved (Figure S6) and, in the USP5 structure, pointed toward the solvent. The opposite face of nUBA interacted weakly with the zinc-ribbon-like subdomain, burying a surface area of about 345 Å^2 involving no hydrogen or ionic bonds. When ubiquitin was docked onto the putative ligand binding face of nUBA, the C-terminal diglycine motif was greater than 30 Å away from the nearest side chain of the active-site-bound proximal S1 (Figure S7) ubiquitin and suggested that it did not interact with the S2 ubiquitin of polyubiquitin substrates. The nUBA likely interacted with the S3 unit of polyubiquitin.

The fact that the cUBA interacted extensively with both the catalytic domain and the bound ubiquitin was intriguing. The cUBA interacted with the loop of the catalytic domain immediately following α11, burying a predominantly aromatic surface area of about 600 Å^2 involving one hydrogen bond (between Arg452 NE and Gly771 O) and one salt bridge (between Arg449 NH and Aps733 OD). The third cUBA helix (α19) also made extensive contacts with the active site-bound S1 ubiquitin, particularly with ubiquitin's long β3−β4 loop, including four hydrogen bonds and three salt bridges (Figure S6). Interestingly, one of these salt bridges was with ubiquitin's Lys48 ε-amino group (NZ), suggesting that if the cUBA was restricted to this position, USP5 would not be able to accommodate K48-linked polyubiquitin-chain substrates longer than two units. Although other S1 ubiquitin lysines were exposed in the structure, when ubiquitin was docked onto the putative ligand binding face of cUBA, the docked ubiquitin made significant clashes with the catalytic domain. Taken together, these observations suggest that the cUBA orientation in this structure may contribute specifically to diubiquitin binding. Nevertheless, the loosely tethered nature of the UBA domains and likely the considerable conformational mobility of the UBA domains relative to the catalytic core is consistent with the fact that USP5 efficiently disassembles multiple types of polyubiquitin chains, including K6-, K11-, K29-, K48-, and K63-linked, and linear chains[6] (Figure 2B).

cUBP. USP5 is an exoisoamidase that cleaves polyubiquitin from the proximal end of the chain (the end that contains the free C-terminal diglycine motif), involving binding of the free C-terminal substrate tail to the cUBP (aka ZnF-UBP).[8] Addition of free monoubiquitin was previously shown to activate ubiquitin-AMC hydrolysis. Because the added free monoubiquitin was not covalently attached to the ubiquitin-AMC, it must not have contributed to an increased affinity for the substrate (in this case, Ub-AMC); instead, it was suggested that the added free monoubiquitin contributed to transition-state stabilization by optimizing (via the cUBP) the orientation of the catalytic triad and nearby active site pocket. Alternatively, unliganded cUBP may have disrupted the active site; addition of free monoubiquitin may have relieved this autoinhibition.

Our full-length USP5 structure showed that although the cUBP was within the vicinity of the catalytic triad, it did not form direct interactions other than a disulfide bridge, which was puzzling (Figure S8A). The cUBP cysteine (Cys195) was also involved in disulfide bridges in both the apo and complex cUBP structures (PDBs 2G43 and 2G45). The fact that these cysteine residues may be readily solvent exposed that the catalytic-side cysteine is not conserved (Figure S1) and that the cUBP cysteine was not necessary for tetraubiquitin hydrolysis (Figure 2A) argued against a role in catalysis and suggested that the interaction between the cUBP and the catalytic domain in this structure was an artifact of crystallization. Indeed, it is possible that this structure does not represent a catalytically competent state. The linkers on either side of cUBP, being disordered and lengthy (17 residues on the N-terminal side and 36 residues on the C-terminal side), would allow for considerable flexibility in the positioning of this domain relative to the catalytic. Finally, docking ubiquitin onto the FL structure according to the cUBP-Ub complex (PDB 2G45) showed that the NZ atom of K48 of the cUBP-Ub complex was ∼45 Å away from the catalytic cysteine (Figure S8B). When we presumed flexibility in the ubiquitin C-tail (residues 70−74) and manually docked ubiquitin to minimize the distance between K48 and the active site without steric clashes, the smallest distance was about 8 Å (Figure S8B). Therefore, the current structure does not readily support a model whereby the cUBP would contribute directly (or allosterically) to the active site and to the catalytic machinery. Neither does it support an autoinhibitory model. Instead, our structure suggests that the cUBP has evolved to adopt a variety of orientations to accommodate a large array of possible substrate chains. The cUBP is part of the extended substrate binding site without contributing directly to the active site. It likely contributes mainly to an increased affinity for polyubiquitin substrates.

nUBP. At the N-terminus of USP5 we discovered a novel domain of 156 amino acids (residues 1−156) comprised of three α-helices surrounding a single antiparallel, five-stranded β-sheet (Figure 1, Figure S1). It adopted a ZnF-UBP fold. The closest structural homologue of this domain, as reported by the DALI server,[26] was human histone deacetylase 6 (PDB: 3C5K) (manuscript in preparation) with an rmsd of 0.67 Å across 98 backbone atoms. The prototypical ZnF-UBP domain is the cUBP of USP5, which tightly binds and buries the free C-terminal ubiquitin tail (the sequence: RGG) through an aromatic pocket; also, a guanidino group from an arginine chain from an abutting loop interacts with the carbonyl groups of Arg74 and Gly75 of ubiquitin.[8] In contrast, this cleft of the novel domain of USP5 (herein called nUBP) was filled by a tyrosine (Tyr128) from the β4-β5 loop and no arginine (Arg221 in cUBP) was present to form potential hydrogen bonds with ligand (Figure 3A). Sequence alignments suggested that filled binding pockets are present in USP20, 22, and 33, and some of them have already been shown to be unable to bind free ubiquitin.[27]

The zinc coordination site in cUBP is comprised of the residue side-chains His232, Cys219, Cys199, and Cys202. While the overall geometry of the corresponding site in nUBP was preserved, only one of the four coordinating residues, Cys33 (corresponding to Cys199 of cUBP) was conserved. Therefore, nUBP did not seem to have a functional Zn^{2+} binding site, and this was supported by the lack of residual and $2F_o - F_c$ electron density in these areas.

Although nUBP was unlikely to bind ubiquitin, we confirmed this experimentally. Pull-down experiments were conducted with mature, N-terminally tagged human modifiers, immobilized on IMAC resin, and either GST-nUBP or untagged cUBP. A series of other modifiers were run in parallel as controls. The

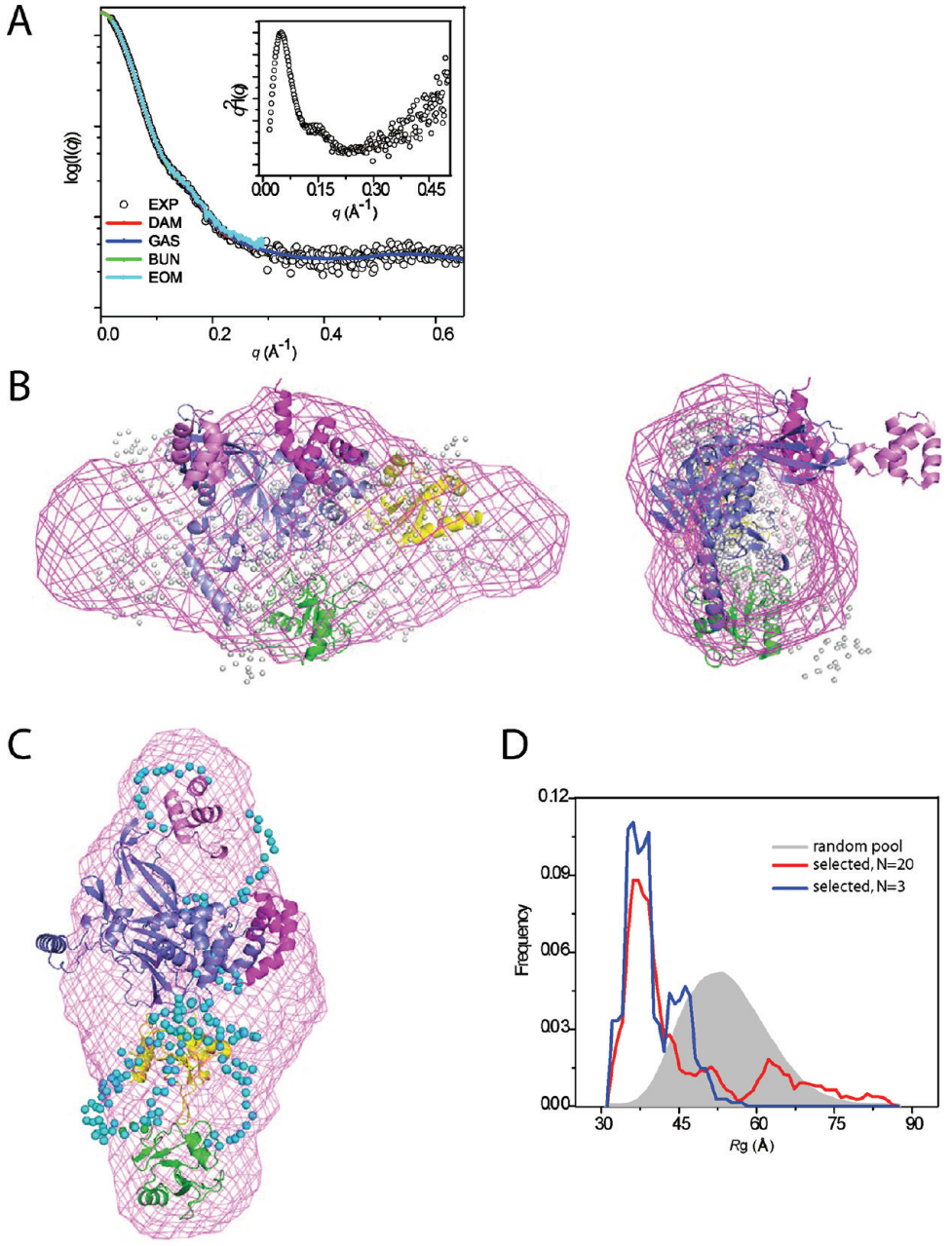

Figure 4. SAXS results for apo-USP5 in solution. (A) Shown are representative fits of the curves from DAMMIN (red), GASBOR (blue), BUNCH (green), and EOM (cyan) to the experimental scattering profile of apo-USP5 (open black circle). The inset shows the Kratky plot ($q^2I(q)$ vs q) of the scattering profile of apo-USP5. (B) Shown is the crystal structure fitted to the *ab initio* envelope generated by DAMMIN (magenta mesh). Also shown is a GASBOR dummy residue model (gray spheres) fitted to the DAMMIN envelope. (C) A representative BUNCH model fitted to the DAMMIN envelope (magenta mesh) is shown; the linkers are displayed as cyan spheres. (D) Distribution of the selected conformers (red to 20 conformers per ensemble and blue to 3 conformers per ensemble) and the initial pool of 10 000 random conformers (gray area) as a function of R_g is shown. The color code for individual domain is the same as those in Figure 1.

cUBP bound well to ubiquitin and ISG15, but no other UBL (Figure S9). ISG15 bound a little less tightly probably because its Leu121 side chain was unable to make a water-mediated hydrogen bond with the Arg221 guanidinium side chain of cUBP. In contrast, the nUBP domain did not interact with either ubiquitin or ISG15. Although ISG15 inhibitors bound to the USP5 catalytic domain,[28,29] our data suggested that unanchored ISG15 may bind to the ZnF-UBP domain. Although ISG15 modified proteins (which do not have a free diglycine moiety) were shown to be USP5 substrates, our data suggested that unanchored ISG15 or ISG15 chains may be also be substrates.

Conserved residues of nUBP were mapped by aligning USP5 sequences available from the NCBI database. Only three residues were fully conserved: Cys30, Gly42, and Leu99. Using the ClustalW server, 20 residues were identified that were partially conserved, many of which when mapped to the nUBP structure corresponded to core residues (buried residues); the few conserved surface residues formed a patch composed mainly of residues 26 to 37 (loop between α1 and β1) and some nearby residues. Interestingly, this α1–β1 loop was

dx.doi.org/10.1021/bi200854q | *Biochemistry* 2012, 51, 1188–1198

Table 2. Kinetic Parameters of Ub-AMC Cleavage Catalyzed by USP5 Variants

USP5 variant	K_m (nM)	k_{cat} (min^{-1})	k_{cat}/K_m (min^{-1} μM^{-1})
wild-type (1−835)	690 ± 3	47 ± 1	68.1
minimal catalytic domain (319−835)	n.d.[a]	n.d.	
ΔnUBP (173−835)	n.d.	n.d.	
ΔcUBP (1−835, Δ172−286)	940 ± 30	5.0 ± 0.1	5.3
nUBP double mutant (1−835, F32S/F34S)	1630 ± 100	0.20 ± 0.01	0.12

[a]n.d., not detectable under assay conditions (see Materials and Methods).

almost completely buried by the catalytic domain, making 723 $Å^2$ of the surface area of the nUBP inaccessible to solvent. Two nUBP phenylalanines (Phe32 and 34) were buried in the catalytic domain, Glu20 and Arg60 in the nUBP formed salt bridges with Lys379 and Glu359, respectively, in the catalytic domain, and His26 and Lys64 in the nUBP hydrogen bonded with Thr370 and the backbone carbonyls of residues 362, 365, and 366, respectively, in the catalytic domain (Figure 3B). These contacts suggested that the interaction between nUBP and the catalytic domain in the structure was tight and may be biologically relevant.

Solution Studies by Small-Angle X-ray Scattering. Small-angle X-ray scattering (SAXS) is a powerful technique for characterizing biological macromolecules in solution. Recently, this technique was successfully used to quantify the conformational ensembles of a number of flexible macromolecules in solution.[30] In order to show that USP5 contained flexible substrate targeting domains and adopted a larger overall volume in solution compared with its crystal structure, we analyzed the structure of apo-USP5 in solution using SAXS. The apparent molecular weight of apo-USP5 estimated from forward scattering $I(0)$ using BSA as a molecular weight standard was 87 ± 10 kDa. This was in agreement with the molecular weight calculated from the primary sequence (95 kDa) and confirmed that apo-USP5 was a monomer in solution. Guinier analysis of the scattering data revealed that apo-USP5 had a radius of gyration (R_g) of 38.2 ± 0.2 Å and a D_{max} of about 145 Å; the latter was determined from calculation of pair distance distribution functions using GNOM (Figure S10). The theoretical scattering curve calculated from the crystal structure using CRYSOL revealed an R_g of 31.5 Å, and the fitting of the theoretical scattering curve to the experimental scattering profile showed a high discrepancy (χ^2 = 15.8) (Figure S10).

From the SAXS data, we generated 32 independent *ab initio* shape models using the DAMMIN program. The mean normalized spatial discrepancy (NSD) score among the models, as calculated by DAMAVER, was 0.65 ± 0.02, and the chi numbers for the fitting of all *ab initio* models to the experimental scattering (q in 0.002−0.3 $Å^{-1}$) (Figure 4A) was in the range of 1.264 ± 0.003, indicating excellent convergence in both individual DAMMIN fits and overall bead model ensembles. Next, 32 *ab initio* models with a higher resolution were generated using GASBOR. The NSD among 32 independent GASBOR models was 1.712 ± 0.043, and all dummy residue models fit to the experimental scattering data (q in 0.002−0.65 $Å^{-1}$) (Figure 4A) with chi numbers in the range 1.356−2.347. The model with the best fitting chi (1.356) is shown in Figure 4B. While the averaged models from DAMMIN (Figure 4B) and GASBOR (not shown) were very similar in overall shape, the relative higher NSD among GASBOR models suggested that finer features of the shape were not consistent between different models, indicating that no single conformation of 835 chainlike dummy residues could satisfy the data. This implied intrinsic flexibility in apo-USP5. Manual fitting of the USP5 crystal structure without ubiquitin into the *ab initio* envelope readily showed that the overall volume of the envelope was larger than the volume of the apo USP monomer in the crystal structure (Figure 4B), even after taking into account the number of unmodeled residues in the crystal structure (160/835 = 19%). But the envelope was not large enough to accommodate a USP5 dimer. Although the envelope was consistent with a centrally located catalytic domain, additional volume in the envelope was observed near the UBA domains and particularly near the nUBP domain (Figure 4B).

Because SAXS data were collected for apo-USP5 under reducing conditions, the cUBP domain may not necessarily have adopted the disulfide-bonded orientation observed in the crystal structure. The Kratky plot of the scattering profile of apo-USP5, shown as inset in Figure 4A, was characteristic of partially folded molecules with flexibility, having bell-shaped peaks at low q range and a slowly increasing curve at large q values. To fit the individual domains to the SAXS data, we carry out rigid body modeling utilizing the BUNCH program to optimize the relative position and orientation of individual domains. A total of eight BUNCH models were generated with chi in the range 2.50−3.71 (Figure 4A). The model with lowest fitting discrepancy had R_g and D_{max} values of 38.1 ± 0.1 and 143 Å, respectively, in good agreement with experimental data (Figure 4C).

To further assess the flexibility of apo-USP5 in solution, we employed the ensemble optimization method (EOM).[22] In this approach, the linkers were allowed to be completely flexible, and the five individual domains were used as rigid domain inputs to generate a pool of 10 000 conformers. A genetic algorithm selection process generated ensembles containing multiple conformers that best fit the experimental scattering curve. The EOM analysis produced a skewed R_g distribution compared with the broad range of R_g exhibited by the initial pool (Figure 4D). For an optimized ensemble with N = 20 conformers and a good fit (chi of 1.58) (Figure 4A), the R_g distribution curve was dominated by a compact population with R_g centered around 40 Å (Figure 4D). However, if only three possible conformers were selected for the calculation, the fitting chi was 1.56, a value comparable to that of N = 20, and the population of slightly extended conformers (R_g ranging 42−57) was enriched (Figure 4D). This strongly suggested that alternative extended conformations other than the dominant compact conformation may be relevant. Importantly, this calculation suggested that USP5 adopted mostly compact structures with a significant population of slightly extended conformers coexisting in solution. In other words, the five individual USP5 domains were not completely flexible relative to each other and interdomain interactions existed among them. The general orientation of the nUBP adjacent to the

catalytic domain observed in the crystal structure likely remained relevant in solution.

Mechanism of Action. Hydrolysis of Ub-AMC by USP5 was previously found to be stimulated by low concentrations of free monoubiquitin.[6,31,32] This suggested one of two potential models of regulation, both of which rely on a two-conformation model. In one model, the unliganded cUBP inhibits catalytic activity of USP5 in one conformation and the liganded cUBP does not inhibit activity in another conformation. In another model, the cUBP contributes allosterically to the catalytic mechanism only when substrate is bound to the cUBP. Our structure did not readily support either of these models. First, the extent of cUBP−catalytic interaction was insignificant if the disulfide bridge was not considered relevant; second, the orientation of the cUBP relative to the catalytic domain was not in a catalytically competent state.

To establish the relevance of the cUBP, deletion of only the cUBP (ΔcUBP) resulted in a mild ∼13-fold lower activity compared with wild-type protein (Table 2). That the k_{cat} but not the K_m was affected was consistent with the fact that the substrate used (Ub-AMC) did not bind to the cUBP and therefore did not contribute to that K_m. A 9-fold reduction in kcat is not substantial in the light of the dramatic effect of the nUBP domain as well as the minimal catalytic domain (residues from 319 to 835), which was multiple orders of magnitude less active than full length (Table 2). Deletion of only the nUBP (ΔnUBP) or substitution with serine of Phe32 and 34, which were buried in the interaction with the catalytic domain, resulted in a dramatic decrease (>1000-fold) in catalytic activity as measured by the Ub-AMC hydrolysis assay (Table 2). The activity data and the crystal structure, when taken together suggested that the effect of nUBP on catalytic activity was allosteric. The presence of nUBP stabilized the enzyme−substrate interaction and also significantly increased enzyme turnover. Whether this domain activates the catalysis of larger substrates and plays a role in substrate selectivity remains to be established. Taken together, these results did not strongly support the hypothesis that the cUBP was autoinhibitory and argued against the model that cUBP contributed directly to the catalytic machinery.

We propose that anchoring of the cUBP through opposite ends of the domain (to the catalytic domain and to the nUBP domain) would allow a range of motion and flexibility compatible with binding different substrate linkages. The cUBP may contribute by increasing affinity for polyubiquitin substrates (decreases the substrate's K_m). The functional role of the nUBP, beyond being required for catalytic activity, and its possible involvement in regulation of USP5 activity or signaling processes, remains to be determined.

SUMMARY

The crystal structure of full length USP5 as well as the low-resolution scattering studies suggested conformational flexibility to accommodate a variety of different types of polyubiquitin substrates. The four ubiquitin-binding domains, cUBP, catalytic, nUBA, and cUBA, loosely interacted with each other and are connected by flexible peptide loops that permit, within certain limits, substantial changes in their relative orientations. Indeed, selective deletion of the cUBP (ZnF-UBP) did not radically affect hydrolysis of ubiquitin-AMC. Interestingly, tight interaction of the newly discovered N-terminal nUBP domain with the catalytic domain may be required to keep the cUBP tethered within proximity of the catalytic domain, providing it an appropriate range of flexibility that matches structural ensembles of different ubiquitin chain substrates.

ASSOCIATED CONTENT

Supporting Information

Figures S1−S10. This material is available free of charge via the Internet at http://pubs.acs.org.

AUTHOR INFORMATION

Corresponding Author

*Ph: 416-946-3876; Fax: 416-946-0588; e-mail: sirano.dhepaganon@utoronto.ca.

Author Contributions

#Equal contributions.

Funding

The Structural Genomics Consortium is a registered charity (number 1097737) that receives funds from the Canadian Institutes for Health Research, the Canadian Foundation for Innovation, Genome Canada through the Ontario Genomics Institute, GlaxoSmithKline, Karolinska Institutet, the Knut and Alice Wallenberg Foundation, the Ontario Innovation Trust, the Ontario Ministry for Research and Innovation, Merck & Co., the Novartis Research Foundation, the Swedish Agency for Innovation Systems, the Swedish Foundation for Strategic Research, and the Wellcome Trust. Y.-X. Wang. and X. Fang are supported by the Intramural Research funds of the National Cancer Institute, National Institutes of Health, Department of the Human Health Service, USA.

Notes

The authors declare no competing financial interest.

ACKNOWLEDGMENTS

Use of the Advanced Photon Source was supported by the U.S. Department of Energy, Office of Science, Office of Basic Energy Sciences, under Contract DE-AC02-06CH11357 and under the Partner User Proposal PUP No. 22978. We thank Drs. S. Seifert and R. E. Winans (BESSRC, sector 12-ID) at Argonne National Laboratory for their support for synchrotron experiments.

ABBREVIATIONS

rmsd, root-mean-square deviation; Ub-AMC, ubiquitin 7-amino-4-methylcoumarin; BisTris, 2-[bis(2-hydroxyethyl)-amino]-2-(hydroxymethyl)propane-1,3-diol; Tris, tris-(hydroxymethyl)amino methane; Hepes, (4-(2-hydroxyethyl)-1-piperazineethanesulfonic acid); NaOAc, sodium acetate; SAXS, small-angle X-ray scattering; R_g, radius of gyration; DTT, dithiothreitol; NH_4SO_4, ammonium sulfate

REFERENCES

(1) Komander, D. (2009) The emerging complexity of protein ubiquitination. *Biochem. Soc. Trans. 37*, 937−953.

(2) Ikeda, H., and Kerppola, T. K. (2008) Lysosomal localization of ubiquitinated Jun requires multiple determinants in a lysine-27-linked polyubiquitin conjugate. *Mol. Biol. Cell 19*, 4588−4601.

(3) Peng, J., Schwartz, D., Elias, J. E., Thoreen, C. C., Cheng, D., Marsischky, G., Roelofs, J., Finley, D., and Gygi, S. P. (2003) A proteomics approach to understanding protein ubiquitination. *Nature Biotechnol. 21*, 921−926.

(4) Bremm, A., Freund, S. M., and Komander, D. (2010) Lys11-linked ubiquitin chains adopt compact conformations and are

preferentially hydrolyzed by the deubiquitinase Cezanne. *Nat. Struct. Mol. Biol. 17*, 939−947.
(5) Fushman, D., and Walker, O. (2010) Exploring the linkage dependence of polyubiquitin conformations using molecular modeling. *J. Mol. Biol. 395*, 803−814.
(6) Wilkinson, K. D., Tashayev, V. L., O'Connor, L. B., Larsen, C. N., Kasperek, E., and Pickart, C. M. (1995) Metabolism of the polyubiquitin degradation signal: structure, mechanism, and role of isopeptidase T. *Biochemistry 34*, 14535−14546.
(7) Reyes-Turcu, F. E., Shanks, J. R., Komander, D., and Wilkinson, K. D. (2008) Recognition of polyubiquitin isoforms by the multiple ubiquitin binding modules of isopeptidase T. *J. Biol. Chem. 283*, 19581−19592.
(8) Reyes-Turcu, F. E., Horton, J. R., Mullally, J. E., Heroux, A., Cheng, X., and Wilkinson, K. D. (2006) The ubiquitin binding domain ZnF UBP recognizes the C-terminal diglycine motif of unanchored ubiquitin. *Cell 124*, 1197−1208.
(9) Wilkinson, K. D., Gan-Erdene, T., and Kolli, N. (2005) Derivitization of the C-Terminus of Ubiquitin and Ubiquitin-like Proteins Using Intein Chemistry: Methods and Uses. *Methods Enzymol. 399*, 37−51.
(10) Minor, W., Cymborowski, M., and Otwinowski, Z. (2002) Automatic system for crystallographic data collection and analysis. *Acta Phys. Pol., A 101*, 613−619.
(11) Collaborative Computational Project. (1994) The CCP4 suite: programs for protein crystallography. *Acta Crystallogr. 50*, 760−763.
(12) Emsley, P., and Cowtan, K. (2004) Coot: model-building tools for molecular graphics. *Acta Crystallogr., Sect. D: Biol. Crystallogr. 60*, 2126−2132.
(13) Painter, J., and Merritt, E. A. (2006) TLSMD web server for the generation of multi-group TLS models. *J. Appl. Crystallogr. 39*, 3.
(14) Konarev, P. V., Volkov, V. V., Sokolova, A. V., Koch, M. H. J., and Svergun, D. I. (2003) PRIMUS: a Windows PC-based system for small-angle scattering data analysis. *J. Appl. Crystallogr. 36*, 1277−1282.
(15) Svergun, D. (1992) Determination of the regularization parameter in indirect-transform methods using perceptual criteria. *J. Appl. Crystallogr. 25*, 495−503.
(16) Svergun, D., Barberato, C., and Koch, M. H. J. (1995) CRYSOL - a Program to Evaluate X-ray Solution Scattering of Biological Macromolecules from Atomic Coordinates. *J. Appl. Crystallogr. 28*, 768−773.
(17) Svergun, D. I. (1999) Restoring low resolution structure of biological macromolecules from solution scattering using simulated annealing. *Biophys. J. 76*, 2879−2886.
(18) Svergun, D. I., Petoukhov, M. V., and Koch, M. H. (2001) Determination of domain structure of proteins from X-ray solution scattering. *Biophys. J. 80*, 2946−2953.
(19) Volkov, V. V., and Svergun, D. I. (2003) Uniqueness of ab initio shape determination in small-angle scattering. *J. Appl. Crystallogr. 36*, 860−864.
(20) Kozin, M. B., and Svergun, D. I. (2001) Automated matching of high- and low-resolution structural models. *J. Appl. Crystallogr. 34*, 33−41.
(21) Petoukhov, M. V., and Svergun, D. I. (2005) Global rigid body modeling of macromolecular complexes against small-angle scattering data. *Biophys. J. 89*, 1237−1250.
(22) Bernado, P., Mylonas, E., Petoukhov, M. V., Blackledge, M., and Svergun, D. I. (2007) Structural characterization of flexible proteins using small-angle X-ray scattering. *J. Am. Chem. Soc. 129*, 5656−5664.
(23) Renatus, M., Parrado, S. G., D'Arcy, A., Eidhoff, U., Gerhartz, B., Hassiepen, U., Pierrat, B., Riedl, R., Vinzenz, D., Worpenberg, S., and Kroemer, M. (2006) Structural basis of ubiquitin recognition by the deubiquitinating protease USP2. *Structure 14*, 1293−1302.
(24) Hurley, J. H., Lee, S., and Prag, G. (2006) Ubiquitin-binding domains. *Biochem. J. 399*, 361−372.
(25) Zhang, D., Raasi, S., and Fushman, D. (2008) Affinity makes the difference: nonselective interaction of the UBA domain of Ubiquilin-1 with monomeric ubiquitin and polyubiquitin chains. *J. Mol. Biol. 377*, 162−180.
(26) Holm, L., Kaariainen, S., Rosenstrom, P., and Schenkel, A. (2008) Searching protein structure databases with DaliLite v.3. *Bioinformatics 24*, 2780−2781.
(27) Allen, M. D., and Bycroft, M. (2007) The solution structure of the ZnF UBP domain of USP33/VDU1. *Protein Sci. 16*, 2072−2075.
(28) Catic, A., Fiebiger, E., Korbel, G. A., Blom, D., Galardy, P. J., and Ploegh, H. L. (2007) Screen for ISG15-crossreactive deubiquitinases. *PLoS One 2*, e679.
(29) Hemelaar, J., Borodovsky, A., Kessler, B. M., Reverter, D., Cook, J., Kolli, N., Gan-Erdene, T., Wilkinson, K. D., Gill, G., Lima, C. D., Ploegh, H. L., and Ovaa, H. (2004) Specific and covalent targeting of conjugating and deconjugating enzymes of ubiquitin-like proteins. *Mol. Cell. Biol. 24*, 84−95.
(30) Bernado, P.; Svergun, D. I. Structural analysis of intrinsically disordered proteins by small-angle X-ray scattering. *Mol. BioSyst.*, in press.
(31) Dang, L. C., Melandri, F. D., and Stein, R. L. (1998) Kinetic and mechanistic studies on the hydrolysis of ubiquitin C-terminal 7-amido-4-methylcoumarin by deubiquitinating enzymes. *Biochemistry 37*, 1868−1879.
(32) Stein, R. L., Chen, Z., and Melandri, F. (1995) Kinetic studies of isopeptidase T: modulation of peptidase activity by ubiquitin. *Biochemistry 34*, 12616−12623.